Marine Micropaleontology 169 (2021) 102051

Contents lists available at ScienceDirect

Marine Micropaleontology

journal homepage: www.elsevier.com/locate/marmicro

Integrated calcareous nannofossil and magnetostratigraphic record of ODP Site 709: Middle Eocene to late Oligocene paleoclimate and paleoceanography of the Equatorial Indian Ocean

Giuliana Villa [a,*], Fabio Florindo [b,c], Davide Persico [a], Pontus Lurcock [b], Ana Paula de Martini [c], Luigi Jovane [c], Chiara Fioroni [d]

[a] Università degli Studi di Parma, Dipartimento di Scienze Chimiche della Vita e della Sostenibilità ambientale, Parco Area delle Scienze, 157 a, 43124 Parma, Italy
[b] Istituto Nazionale di Geofisica e Vulcanologia, Via di Vigna Murata 605, Roma 00143, Italy
[c] Instituto Oceanográfico, Universidade de São Paulo, Praça do Oceanográfico, 191, SP 05508-120 São Paulo, Brazil
[d] Università degli Studi di Modena e Reggio Emilia, Dipartimento di Scienze Chimiche e Geologiche, Via Campi, 103, 41125 Modena, Italy

ARTICLE INFO

Keywords:
Calcareous nannofossils
Eocene
Oligocene
Biomagnetostratigraphy
Paleoceanography
ODP Site 709

ABSTRACT

We investigated the calcareous nannofossil biostratigraphy and magnetostratigraphy of middle Eocene – lower Oligocene sediments from ODP Hole 709 C, equatorial Indian Ocean.

The new bio-magnetostratigraphic analyses have resulted in an accurate biochronology of the interval spanning Chrons C20r (middle Eocene) to C12r, in which 29 bioevents were investigated, in a 12 myr interval. The magnetostratigraphic signal is less clear across the Eocene-Oligocene transition (EOT) but becomes more reliable at the top of Chron C13n to Chron C12r (early Oligocene). Quantitative analyses of calcareous nannofossil assemblages allowed recognition of the Middle Eocene Climatic Optimum (MECO) and the long cooling trend leading to the glacial state starting in the early Oligocene. We identify two hiatuses, in the lower middle Eocene and across the Eocene-Oligocene Transition (EOT).

Across the latter unconformity, a major transition from oligotrophic to eutrophic favoring nannofossil taxa highlights the enhanced sea surface nutrient availability during the transition to the early Oligocene glacial system. Finally, a late Oligocene warming event is recorded at this site by the increase in calcareous nannofossil taxa that preferred warm water.

1. Introduction

Earth's climate underwent a distinct cooling trend from the early-middle Eocene to early Oligocene, with the emplacement of continental ice sheets on Antarctica (~34 Ma) (Francis et al., 2009; Liu et al., 2009; Bijl et al., 2013). This trend toward the cooler climate was punctuated by transient warming periods, of which the more prominent is the Middle Eocene Climatic Optimum (MECO; ~40 Ma) (Bohaty and Zachos, 2003; Jovane et al., 2007; Villa et al., 2008; Bohaty et al., 2009; Westerhold et al., 2020). The transition to glacial conditions, with the formation of a large and permanent East Antarctic Ice Sheet (EAIS), has been linked to a number of causes such as the opening of the Southern Ocean (SO) gateways (Kennett, 1977; Lagabrielle et al., 2009; Sarkar et al., 2019), which led to thermal isolation of Antarctica, the drawdown of pCO_2 (DeConto and Pollard, 2003; Pagani et al., 2005, 2011; Goldner et al., 2014; Kennedy-Asser et al., 2019), and/or a favorable orbital configuration which induced an insolation minimum (Coxall et al., 2005; Pälike et al., 2006).

The Eocene-Oligocene transition (EOT, described by Coxall and Pearson, 2007, and recently reviewed in detail by Hutchinson et al., 2021) encompasses the transition from a greenhouse to an icehouse world, and is characterized by a sudden and sizeable positive change in oxygen isotopic ($\delta^{18}O$) values of benthic foraminifera (Miller et al., 1987; Coxall and Wilson, 2011; Westerhold et al., 2020). This interval is also associated with a perturbation of the carbon cycle, an increase of primary productivity, a 1 km deepening of the Carbonate Compensation Depth (CCD) (Van Andel, 1975; Coxall and Pearson, 2007; Pälike et al., 2012), and a sea-level drop (Miller et al., 2008). A biotic turnover is also recorded in association with the EOT, both in terrestrial (Hooker et al., 2004; Zanazzi et al., 2007) and in marine realms (Wade and Pearson,

* Corresponding author.
E-mail address: giuliana.villa@unipr.it (G. Villa).

https://doi.org/10.1016/j.marmicro.2021.102051
Received 11 January 2021; Received in revised form 8 July 2021; Accepted 30 August 2021
Available online 4 September 2021

2008; Dunkley Jones et al., 2008; Cotton and Pearson, 2011; Villa et al., 2014). These changes have been recorded in several oceanic sites at both high and low latitudes, but data are scarce from the western Indian Ocean.

ODP Leg 115 was drilled in the Indian Ocean (Backman et al., 1988) to obtain a south-north bathymetric transect, to investigate the Réunion volcanic system, and to record the Paleogene to Quaternary stratigraphy. Site 709 was the shallowest core drilled in the transect, and sediments were deposited well above the average CCD during the time interval considered in this work (Touchard et al., 2003).

Through high-resolution quantitative calcareous nannofossil biostratigraphy and new magnetostratigraphic analyses, we compared the results with previous studies carried out in this region (Fioroni et al., 2015; Jones et al., 2019) and constructed a detailed middle Eocene-early Oligocene biochronology for the Equatorial Indian Ocean. In addition, calcareous nannofossils, as previously used to identify ocean latitudinal temperature gradients and productivity (Wei et al., 1992; Aubry, 1992, 1998; Bralower, 2002; Gibbs et al., 2006; Kalb and Bralower, 2012), enabled us to reconstruct the paleoclimatic and paleoceanographic conditions through changes in the assemblages (e.g., Bralower, 2002; Persico and Villa, 2004; Villa et al., 2008; Villa et al., 2014) within a biomagnetostratigraphic framework.

2. Material and methods

Site 709 is located in the western equatorial Indian Ocean at 3°54.9′S and 60°33.1′E at a modern water depth of 3038.2 m on the Madingley Rise, a local topographic high between the Mascarene Plateau and the Carlsberg Ridge (Fig. 1) (Backman et al., 1988). Three holes were cored at this site, recovering a particularly homogeneous section of nannofossil ooze and chalk that ranges in age from the Eocene to the Holocene. The estimated seafloor paleodepth at Site 709 during the middle Eocene through the early Oligocene is 2200 m (Bohaty et al., 2009). Sediments generally have a high carbonate content ($CaCO_3$ wt%) ranging from about 85% to about 94%; a few samples have lower values. Hole 709C was cored to 353.7 m below sea floor (mbsf), with a 93% recovery and ended in nannofossil chalks of middle Eocene age (Backman et al., 1988).(

2.1. Calcareous nannofossils

Micropaleontological analyses were performed on 140 samples, from the working half of the split core Section 709C-29X-1, 28–29 (266.68 mbsf) to Section 709C-37X-7, 12–14.5 (353.13 mbsf) (Appendix A). Sample resolution was approximately 20 cm from middle Eocene to early Oligocene, corresponding to a minimum temporal resolution of about 50 kyr, but was lower in intervals with core disturbance. An upper Oligocene set of 17 samples (from Section 709C-28X-3 to Section 709C-22X-2) was taken at a lower resolution for paleoecological investigations.

Smear slides were prepared from unprocessed samples, following the standard technique (Bown and Young, 1998), and quantitative analyses were conducted under a light microscope at 1250× magnification on a Zeiss Axioscope 40. For each sample at least 300 specimens were counted and classified (Villa et al., 2008) and two additional long traverses were scanned in order to identify rare taxa. The absolute abundance of each taxon was estimated by normalizing the number of the observed specimens to an area of 1 mm^2 (Rio et al., 1990), then plotted versus depth. The number of specimens per mm^2 was used as an indicator of the total abundance of nannofossils in each sample.

The position of biozonal boundaries was calculated as the midpoint between two consecutive samples. The bioevents are indicated here as B

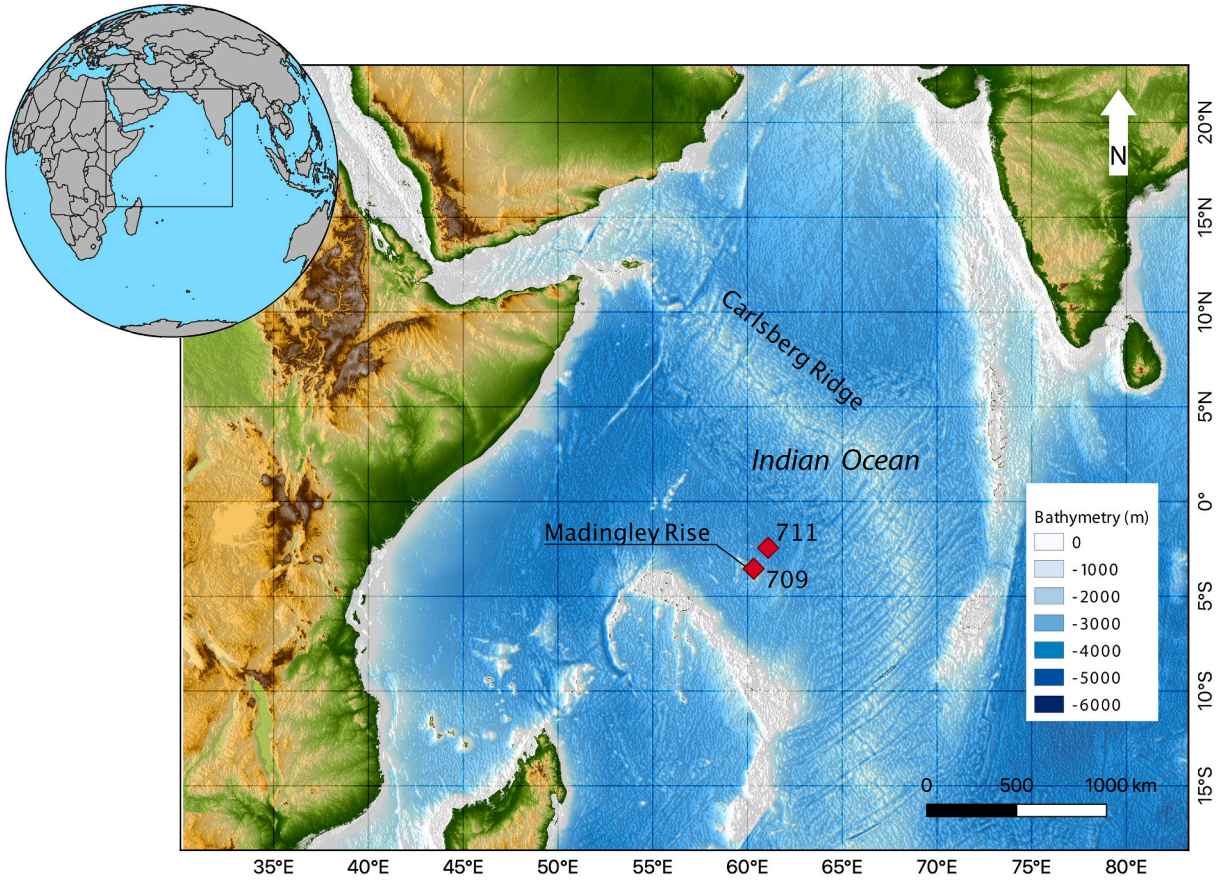

Fig. 1. Location of the studied site (ODP Site 709) and of the nearby ODP Site 711.

(Base, lowest occurrence of the considered taxon), Bc (Base common, common and continuous presence of a taxon), T (Top, highest occurrence of a taxon), Tc (Top common) following Backman et al. (2012).

Nannofossils are usually well preserved but overgrowth is pronounced for some species (e.g., *Discoaster* spp., *C. floridanus*), while other show weak dissolution (e.g., *Helicosphaera* spp.). Reworking is common in some intervals [e.g., 115-709C-29, 115-709C-32 (upper middle Eocene), and 115-709C-33 (lower Oligocene)], but it is negligible in others.

The percentage abundances of the different taxa were used to interpret the assemblage variation in terms of paleoecological changes, since their quantitative analysis is a key proxy for paleoceanographic reconstruction (Winter and Siesser, 1994; Gibbs et al., 2006; Kalb and Bralower, 2012; Villa et al., 2014). Taxa with eutrophic affinities were separated from those with warm/oligotrophic preferences (following Villa et al., 2014 and Fioroni et al., 2015). This allowed the nannofossil species to be grouped with the same paleoecological preference. These values were then plotted against depth to examine stratigraphic changes. Groups include only taxa with well-known paleoecological preferences (Gibbs et al., 2006; Dunkley Jones et al., 2008; Villa et al., 2014; Fioroni et al., 2015; Jones et al., 2019). The warm-water taxa group comprises *Discoaster* spp., *E. formosa,* and *Sphenolithus* spp.; the oligotrophic taxa group includes *Discoaster* spp., and *E. formosa;* the eutrophic taxa group consists of *R. daviesii*, *C. floridanus,* and *Reticulofenestra* spp. (i.e. *R. dictyoda, R. samodurovi,* and *R. umbilicus*) (Table 1).

2.2. Paleomagnetism

Twenty-one advanced piston corer (APC) cores from Hole 709A, nine cores from Hole 709B and thirteen cores from Hole 709C were measured during the ODP cruise with the shipboard pass-through cryogenic magnetometer. The results were described as "erratic paleomagnetic data" and it was not possible to determine the reversal stratigraphy (Shipboard Scientific Party, 1988). Subsequently, Schneider and Kent (1990) investigated additional intervals from Site 709 where they reported that the results were of poor quality. They were able to determine a magnetostratigraphic record for two small intervals along the retrieved succession; from ca. 15 to 35 mbsf (Pliocene-Pleistocene age) and from ca. 170 to 200 mbsf, near the Oligocene-Miocene boundary.

For this study, we collected one hundred and six oriented 7-cc plastic cubes at the Integrated Ocean Drilling Program (IODP) Kochi Core Center, Japan. All samples were taken from the working half of the split core sections 709C-31X-1 to -37X-7 (middle to late Eocene in age) between depths of 286.08 and 353.13 mbsf. We collected a second set of samples up to 266.7 mbsf to extend the analysis into the Oligocene portion of the hole. Both sets of samples were oriented only with respect to vertical, therefore absolute paleomagnetic declinations could not be recovered for the polarity zonation.

Magnetic analyses were performed at the Istituto Nazionale di Geofisica e Vulcanologia (INGV) in Rome. Natural and artificial magnetizations were measured using a narrow-access pass-through 2-G Enterprises cryogenic magnetometer, with in-line alternating field (AF) demagnetization capability, housed in a magnetically shielded room. After measurement of the NRM, samples were demagnetized at successive peak AFs of 5, 10, 15, 20, 25, 30, 35, 40, 50, 60, 80 mT.

The stability of the natural remanent magnetization (NRM) was assessed using vector component diagrams (Zijderveld, 1967). Characteristic remanent magnetization (ChRM) directions were determined using principal component analysis (PCA) with linear best fits calculated from 3 or more demagnetization steps using the PuffinPlot paleomagnetic analysis application (Lurcock and Florindo, 2019).

Following AF demagnetization of the NRM, low-field magnetic susceptibility (κ) was measured using an AGICO KLY-2 Kappabridge magnetic susceptibility meter with a field of 0.1 mT at a frequency of 470 Hz. An anhysteretic remanent magnetization (ARM) was imparted using a

Table 1
Calcareous nannofossil biohorizons identified at Hole 709C.

Bioevent	Mean depth mbsf	Min depth mbsf	Max depth mbsf	AGE (MA) this work	AGE (MA) Agnini et al., 2014	GPTS (1. Cande and Kent, 1995; 2. Pälike et al., 2006)	Tie points
TOP *R. umbilicus*	268.74	268.4	269.08		32.02	2	
TOP *E. formosa*	272.5	272.1	272.9		32.02	2	
BASE *S. akropodus*	281.45	281.2	281.7				
BC *Clausicoccus* spp.	282.73	282.56	282.9		33.88 (*C. subdistichus*)	2	
TOP *D. saipanensis*	285.02	284.1	285.95	hiatus			
BC *R. daviesii*	285.02	284.1	285.95	hiatus			
BC *S. predistentus*	285.02	284.1	285.95	hiatus			
TC *D. barbadiensis*	285.02	284.1	285.95	hiatus			
TC *C. reticulatum*	285.02	284.1	285.95	hiatus			
BC *C. isabellae*	294.73	293.74	295.73	36.9		2	
TC *C. erbae*	296.1	295.9	296.3	37.47		2	
TOP *C. grandis*	300.56	300.4	300.73	38.1		2	
TOP *S. obtusus*	300.56	300.4	300.73	38.1		2	
BC *C. erbae*	301.38	301.15	301.62	38.15		2	
TOP *S. runus*	309.64	309.83	309.45	39.55		2	
BASE *S. obtusus*	312.44	312.19	312.7	39.73		2	
BASE *D. bisectus*	313.91	312.93	314.9	low recovery interval			
TOP *S. spiniger*	313.91	312.93	314.9	low recovery interval			
TOP *S. furcatolithoides*	315.26	315.12	315.4	40.51	40.51 (*S. furc.* Type B)	2	X
TOP *S. strigosus*	316.61	316.47	316.75	40.6		2	
BASE *S. predistentus*	319.03	318.9	319.16	40.95		2	
BC *C. reticulatum*	323.13	322.86	323.4	42.37	42.37	2	
TOP *Nannotetrina* spp.	327.64	327.55	327.73	42.52		2	
BC *R. umbilicus*	327.91	327.73	328.1	42.52		2	X
BASE *S. strigosus*	345.48	345.07	345.9	43.82		1	
BASE *S. runus*	347.08	346.77	347.4	43.86		1	
TOP *S. kempi*	348.71	348.37	349.06	43.9		1	
TOP *P. gigas*	350.8	350.51	351.1		43.96	1	X

0.05 mT direct current (DC) bias field superimposed on a 100mT peak AF and by translating samples through the AF and DC coil system at 10 cm/s, which is the lowest speed allowed by the control software.

Continuously monitored temperature dependence of the low-field magnetic susceptibility (κ) on a few milligrams of powdered samples (up to 700 °C) was performed at the Instituto Oceanográfico da Universidade de São Paulo, Brazil. This was measured in air using a KLY-4 (AGICO) furnace-equipped Kappabridge, in order to determine the characteristic Curie or Néel temperatures of magnetic minerals (Hrouda, 1994). The thermomagnetic curves were analyzed using the Cureval8 program (http://www.agico.com).

2.3. Multivariate analyses on calcareous nannofossil assemblages

Using number of nannofossils/mm^2, dominance and species diversity (H Shannon-Wiener) were calculated by means of the PAST software (Hammer et al., 2001).

Multivariate R-mode Principal Component Analysis (PCA) was performed on the same quantitative database (nannofossils/mm^2) previously converted to natural logarithm, because percentage counts represent a closed set.

We identified the major components of the nannofossil assemblage using PCA. We graphically plotted the factors that explain the maximum variance, and we draw on paleoecological interpretation from these relationships. The interpretation of the factors and their comparison with the abundance curves of the species allow the interpretation of the paleoecological behaviors of the nannofossil species in the stratigraphic sequence. This interpretation, combined with reference data from Villa et al. (2014) and Fioroni et al. (2015), allowed us to subdivide the assemblage into paleoecological groups of species, as already described in Section 2.1.

3. Results and discussion

3.1. Biohorizons

Previously published papers on nannofossil biostratigraphy of Site 709 were presented respectively by Okada (1990) for the Paleogene and Quaternary interval, and by Fornaciari et al. (1990) for the Oligo-Miocene interval. Here we provide a new high resolution biostratigraphic framework based on calcareous nannofossils spanning from about 43.96 Ma (Top of *Pletolithus gigas,* Agnini et al., 2014, Cappelli et al., 2020) to 32.02 Ma (Top of *Reticulofenestra umbilicus,* Agnini et al., 2014) and thus covering ca. 12 myr.

Comparing our results with the nearby Site 711 (Fioroni et al., 2015) provides the opportunity to test the local reliability of the main biohorizons. However, the magnetostratigraphic data available at Site 711 has a low resolution because of the high number of samples (66% of the analyzed samples) with no reliable magnetic directions (Savian et al., 2013). At Site 709, magnetostratigraphic results are more detailed and accurate, and thus suitable to construct a reliable age model and determine correlations on a global scale.

The distribution patterns of the main bioevents plotted against depth are summarized in Fig. 2 and the index species documented in Plate 1. A detailed discussion on each identified bioevent is available in Appendix B.

3.2. Paleomagnetic behavior

NRM intensity ranges between 9.4×10^{-5} and 4.4×10^{-3} A/m with an average of 7.6×10^{-4} A/m. Two higher intensity intervals are located at 296.8 and at 308.7 mbsf (Fig. 3). Downcore variations in NRM intensity and directions are not associated with variations of the concentration-dependent magnetic parameters κ and ARM (Figs. 3, 4).

Stepwise AF demagnetization enabled isolation of the ChRM component for 95% of the samples analyzed, with maximum angular deviation (MAD) values between 0.81 and 10.6. Typical demagnetization behavior is shown in Fig. 4. Most of the samples have a low-coercivity, normal polarity overprint that was successfully removed at peak fields of 10 mT. We interpret this overprint to have been acquired, as an isothermal remanent magnetization, during the drilling process and/or storage (e.g., Fuller et al., 1998). From observations made onboard, Schneider and Kent (1990) reported the presence of a remagnetization induced by the magnetized core barrels that mostly affected the external portions of the cores.

The ChRM inclinations enable delineation of magnetozones, which are defined, in most cases, using at least two consecutive samples with inclinations distinctly different from neighboring intervals (Fig. 5). In some magnetozones, occasional isolated samples have polarities opposite to those of the rest of the magnetozone (e.g., 298.28 mbsf, 322.48 mbsf). Such isolated samples were used with caution to define magnetozones and their correlation with the geomagnetic polarity time scale (GPTS) was inferred by integrating biostratigraphic data.

The observed ChRM inclinations are steeper than the present-day geocentric axial dipole (GAD) inclination (±7.06°) at the site latitude and steeper than the expected GAD paleoinclination (±4°) considering the calculated mean paleolatitude (2.9°S, ±2.8°) of Hole 709C at 40 Ma (Torsvik et al., 2012; van Hinsbergen et al., 2015). A similar inconsistency with the GAD predictions is present in the results obtained at nearby ODP Site 711 by Savian et al. (2013). The authors interpreted this discrepancy as being due to some unresolved combination of unaccounted for motion of the plate, long-term non-dipole fields, and effects of hotspot motion on the plate circuit models. With the available data we cannot rule out that the discrepancy may be related to an unremoved overprint (e.g., Bowles, 2007).

Mean ChRM inclinations were computed separately for normal and reverse polarity populations using the Arason-Levi inclination-only algorithm (Arason and Levi, 2010) as implemented in the PuffinPlot application (Lurcock and Florindo, 2019). The normal polarity samples and the reverse polarity samples have a mean inclination of −36.3° ($N = 39$; $\alpha_{95} = 8.1°$) and 41.8° ($N = 64$; $\alpha_{95} = 5.4°$), respectively. These values very narrowly fail an inclination-only reversals test at the 95% confidence level (since the antipode of the mean normal inclination lies 0.1° outside the 95% cone of confidence for the mean reversed direction), but the marginal nature of this result suggests that the mean directions could indeed represent a reliable polarity record.

3.2.1. Magnetic properties

Magnetic properties do not show substantial changes along the studied interval. The magnetic susceptibility ranges between -16×10^{-5} and 154×10^{-5} SI with a mean of 61.6×10^{-5} SI. The ARM, which is acquired by stable single domain magnetite, shows an average value of 6.8×10^{-3} A/m and ranges between 3.2×10^{-3} and 1.2×10^{-2} A/m (Fig. 3). The relative stability of magnetic susceptibility and ARM suggests that this record does not have significant variations in magnetic mineral concentration.

Continuous monitoring of κ-*T* changes shows a change in slope (albeit noisy) at approximately 580 °C. This suggests the ubiquitous presence of Fe spinels with a composition similar to magnetite (Fig. 3). The behavior of the discrete samples during AF demagnetization (Fig. 4) provides additional support for the presence of magnetite as the main magnetic carrier.

The observed increases in κ during heating are probably due to the thermally induced growth of new magnetite from iron-bearing clays (e.g., Hirt et al., 1993). The cooling curve has higher overall κ than the heating curve, which indicates production of new magnetic phases during heating.

3.3. Age model and magnetobiochronology

We provide an interpretation of the magnetic polarity pattern of Hole 709C from 266.7 to 353.13 mbsf, using the nannofossil bioevents

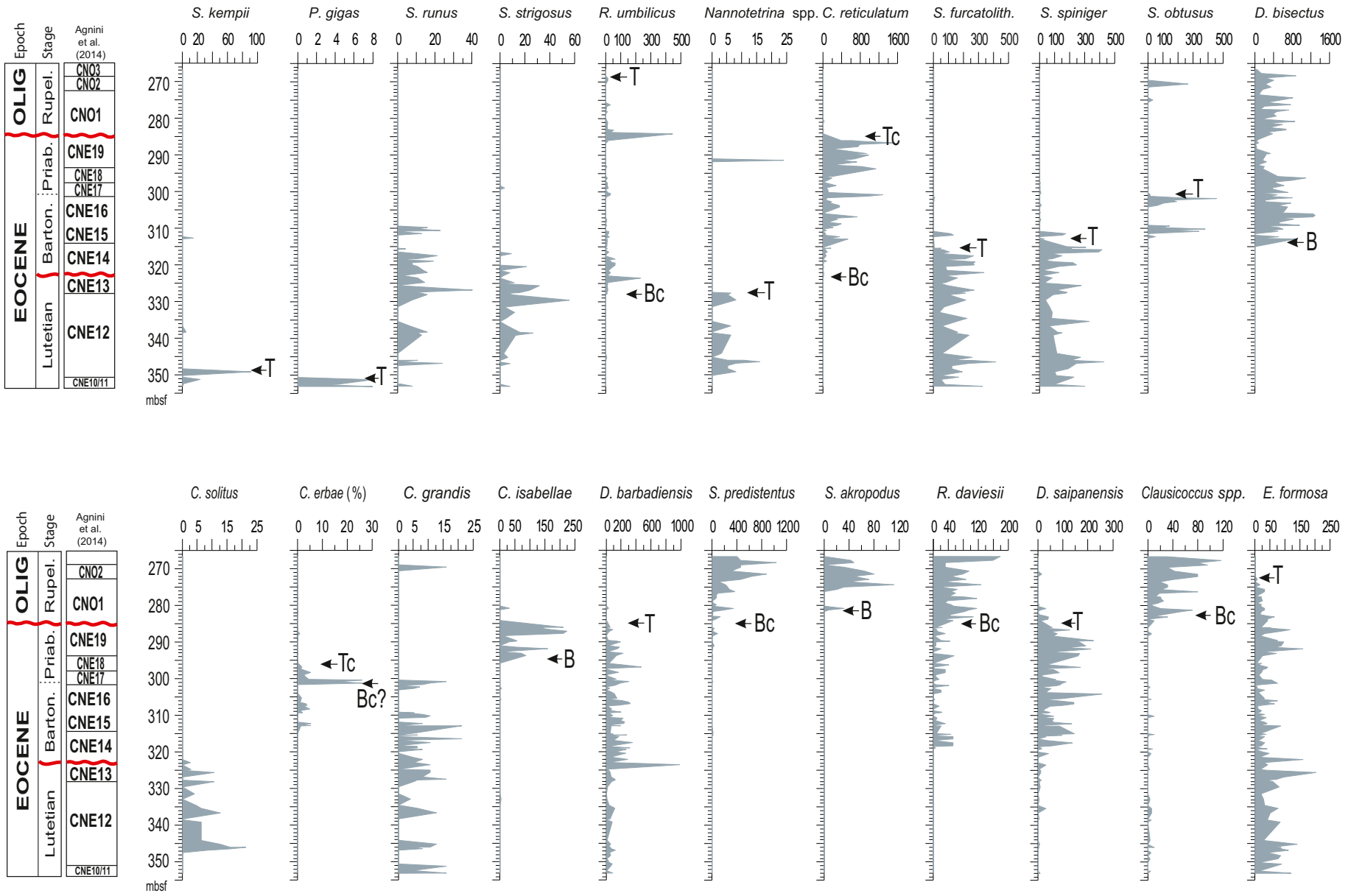

Fig. 2. Abundance patterns of calcareous nannofossil index species at ODP Site 709 plotted against depth (mbsf), the zonation of Agnini et al. (2014), and expressed as number of specimens/mm^2. *C. erbae* is expressed as %, following Fornaciari et al., 2010.

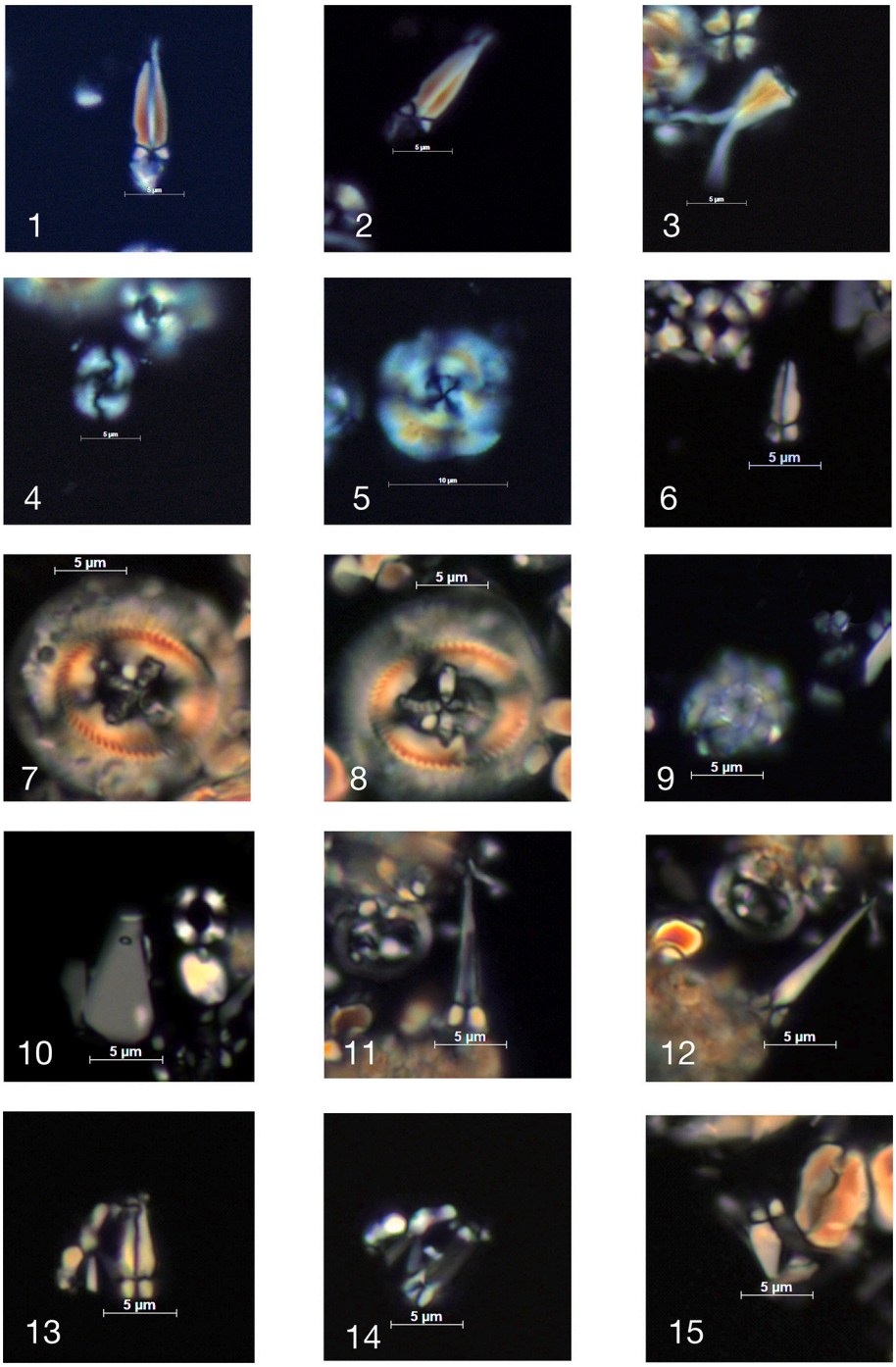

Plate 1. Photomicrographs of selected calcareous nannofossils from Site 709, light microscope, cross-polarized light, 1250× magnification. Figs. 1, 2: *Sphenolithus akropodus*, sample 29 5 50; Fig. 3: *Sphenolithus predistentus*, sample 30 1 138; Fig. 4: *Reticulofenestra daviesii*, sample 30 5 46; Fig. 5: *Cribrocentrum isabellae*, sample 31 5 90; Fig. 6: *Sphenolithus obtusus*, sample 33 3 135; Fig. 7: *Pletolithus gigas*, sample 35 5 70; Fig. 8: *Pletolithus gigas*, sample 36 2 110; Fig. 9: *Discoaster bifax*, sample 35 5 70; Fig. 10: *Bramletteius serraculoides*, sample 30 5 70; Figs. 11, 12: *Sphenolithus runus*, sample 36 3 130; Fig. 13, 14: *Sphenolithus strigosus*, view at 0° and 45°; sample 36 3 130; Fig. 15: *Sphenolithus furcatolithoides*, view at 45°; sample 37 4 56.

observed throughout the section. Following the methodology proposed by Pälike et al. (2010) and applied by Agnini et al. (2014), the bioevents and the interpretation of the magnetic polarity pattern are calibrated against the orbitally tuned time scale of Pälike et al. (2006) from the base of Chron C12r (33.157 Ma) to the base of Chron C19n (41.510 Ma), and with the GPTS of Cande and Kent (1995) between the top of Chron C20n (42.536 Ma) and the base of Chron C20r (46.264 Ma). The age-depth plot and the magnetobiostratigraphic framework are presented in Figs. 6 and 7, respectively.

The combined bio- and magnetostratigraphy results highlight at least two relevant hiatuses. The first hiatus is located between Chron C19r and Chron C18r and the single normal polarity sample at 322.48 mbsf could represent a portion of Chron C19n. The presence of the lower part of Chron C19r at 328.37 mbsf is confirmed by the Bc of *Cribrocentrum reticulatum* at 323.13 mbsf, just below the hiatus. The hiatus represents at least 1 myr of missing time, from the Bc of *C. reticulatum* (aged at 42.37 Ma by Agnini et al., 2014) to the top of Chron C19n (41.358 Ma according to Pälike et al., 2006). A second hiatus, at ca. 285 mbsf, is highlighted by the concurrent extinctions of *Discoaster barbadiensis*, and *D. saipanensis,* whose Tops are at 34.77 Ma, and at 34.44 Ma respectively, *C. reticulatum* (Top at 35.24 Ma, according to Agnini et al., 2014), and *Cribrocentrum isabellae* (Fornaciari et al., 2010) (Figs. 2, 6). Based on calcareous nannofossil data, this hiatus spans Zone CNE20. In addition, at Site 709 just above the hiatus, a noticeable increase in *Clausicoccus* spp. is documented (Fig. 2; Appendix B). Due to overgrowth, specimens of this genus were not recognized at the species level. Based on the mean

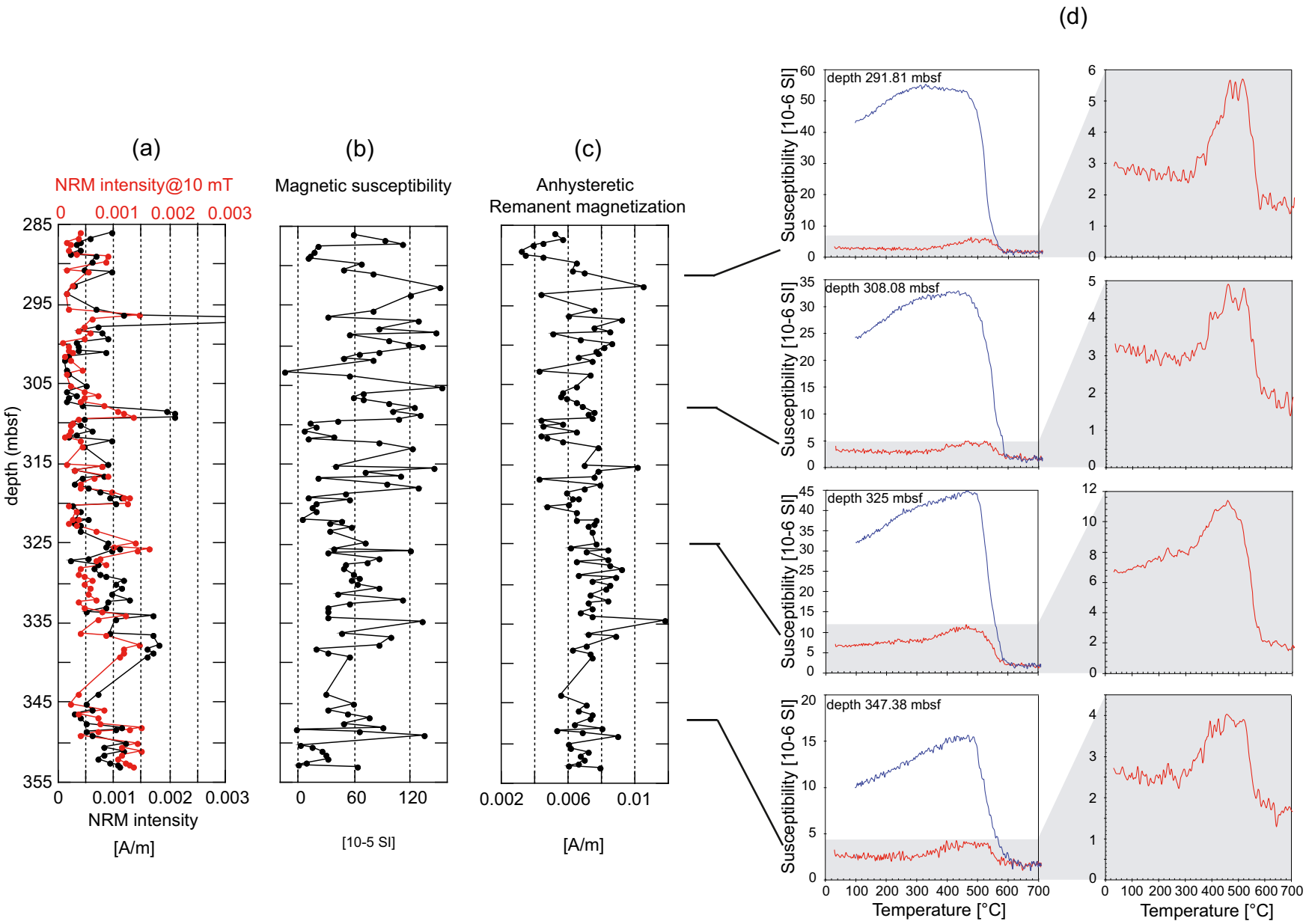

Fig. 3. Stratigraphic variations of intensity of (a) NRM and NRM@10mT, (b) k, (c) ARM and (d) Temperature dependence of κ (up to 700 °C) for four representative samples.

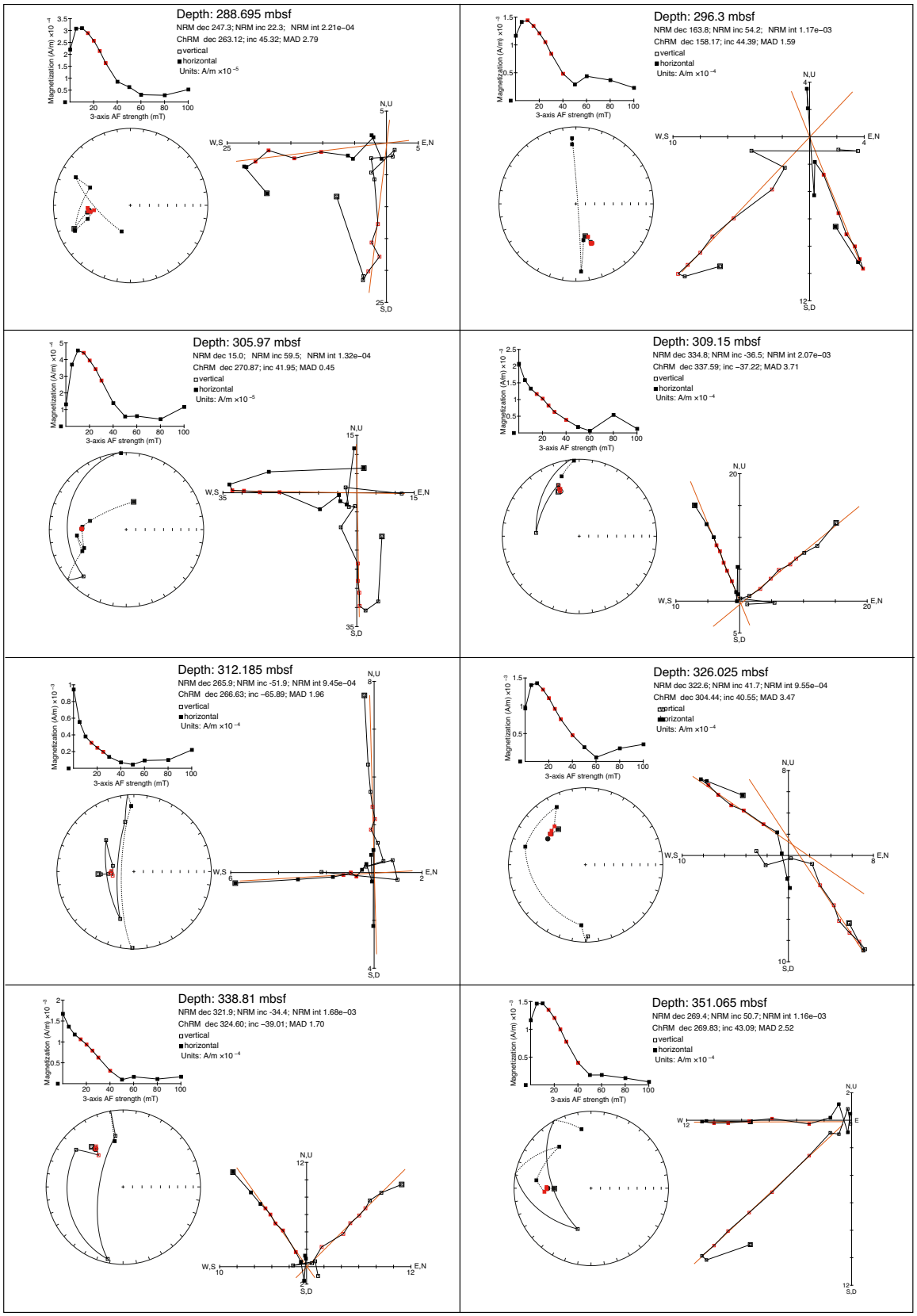

Fig. 4. AF (alternating field) demagnetization behavior for 8 representative samples from Hole 709. For the vector component diagrams, open (closed) symbols represent projections onto the vertical (horizontal) plane. The stereoplots are equal-area projections, with solid (open) symbols representing points projected onto the lower (upper) hemisphere. The cores were not azimuthally oriented; declinations are reported in the laboratory coordinate system with respect to the split face of the core. Plots were produced using PuffinPlot (Lurcock and Florindo, 2019).

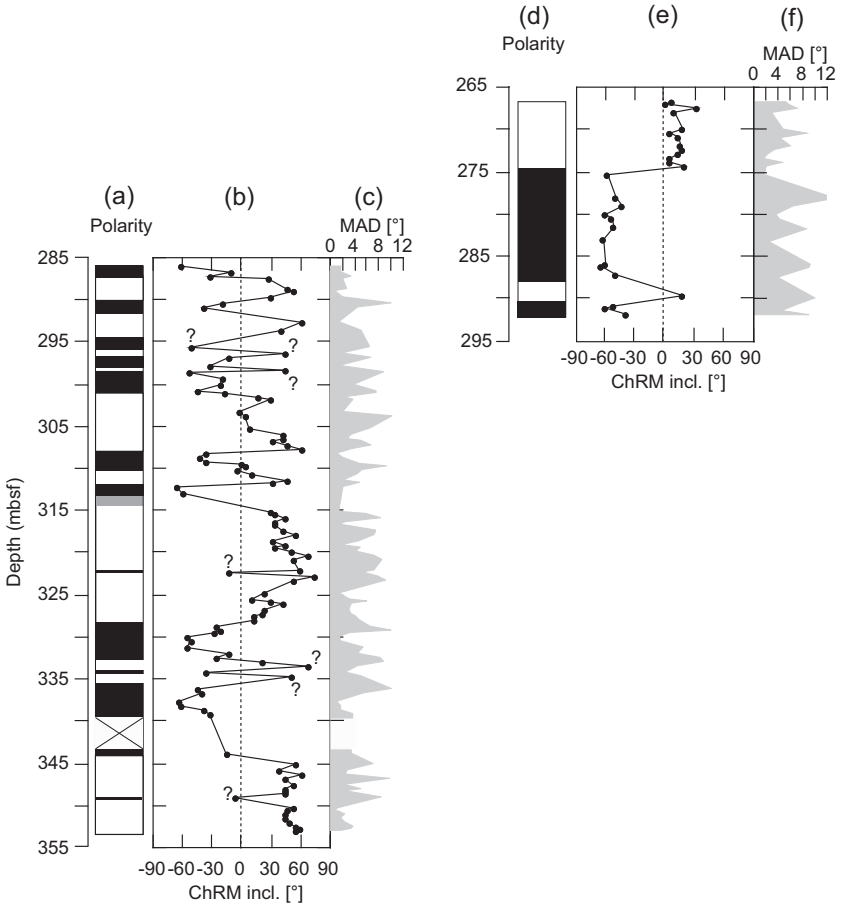

Fig. 5. (a) Magnetic polarity zonation (black = normal polarity and white = reverse polarity), (b) downcore variations of ChRM inclination, (c) MAD. Additional samples collected up to a depth of 266.7 mbsf and analyzed at the Laboratório de Paleomagnetismo of Universidade de São Paulo, Brasil: (d) Magnetic polarity zonation (black = normal polarity and white = reverse polarity), (e) downcore variations of ChRM inclination, (f) MAD.

size of the specimens, however, we are confident that the group is mainly composed of *C. subdistichus*. The beginning acme of this species is reported to have occurred at 33.88 Ma, indicating the base of Zone CNO1 (Agnini et al., 2014) and suggesting that the unconformity also includes Zone CNE21. In contrast, at the nearby Site 711, the nominate bioevents (i.e., *Discoaster* spp., *C. reticulatum*, and *Clausicoccus* spp.) occur stratigraphically close to each other, but are clearly spaced (Fioroni et al., 2015). At Site 711, the availability of a good magneto-stratigraphic record during this time interval confirms these data (Savian et al., 2013); in particular, the Top of *C. reticulatum* is recorded in Chron C15n, whereas the top of the "rosette shaped" *Discoaster* group is recorded in Chron C13r.

The presence of hiatuses at Site 709, unlike the continuous and relatively more expanded record at Site 711, is possibly explained by the more effective role played by the bottom paleocurrents at a shallower depositional setting of this site.

3.4. Multivariate analysis

The interpretation of the PCA factors is based on graphic comparison with the paleoecologically sensitive taxa (Figs. 8, 9) . The indices show fairly stable values from the base up to about 292 mbsf. At this depth, the dominance index and H Shannon-Wiener diversity index show, respectively, increasing and decreasing trends, revealing a change typical of an environmental condition variation. The general trend toward a decline in specific diversity suggests a cooling trend from the middle Eocene to the early Oligocene (Bown et al., 2008; Cronin and Cronin, 2015).

The PCA analyses of the census data show that two significant principal components (PCA1 and PCA2) explain 77% of the variance (Fig. 9). The PC1 scores (PC1, 61.77% of the variance) display a clear shift from negative to positive values at 320 mbsf, at the base of C18r (41.358 Ma) (Fig. 9). This trend is interrupted only at 315 mbsf by a short negative peak, dated at about 40 Ma, that also correlate to a shift in warm-water taxa value. The overall PC1 trend is reminiscent of the $\delta^{18}O$ records from several sites indicative of the paleoclimate evolution of the middle Eocene (Bohaty et al., 2009). Therefore, we associate PC1 with the paleoclimatic factor SST. The positive shift at 320 mbsf should therefore correspond to the pre-MECO cooling event (Bohaty et al., 2009; Savian et al., 2016). We interpret the negative peak at 315 mbsf, as likely coinciding with the MECO, while upward, cooling conditions prevailed.

The PCA factor 2 (PC2, 15.39% of the variance) is dominated by positive scores up to 287 mbsf where it records an abrupt change to negative values. Based on the correlation with diversity and oligotrophy versus eutrophic taxa, we interpret this index to indicate trophic conditions of the surface waters (see § 3.5.3).

3.5. Response of nannofossil abundance to middle Eocene - late Oligocene climate variability

The paleoecological interpretation is based on the relative abundance of the key taxa and on groups of taxa with the same preference treated with a statistical approach (Figs. 8, 9).

3.5.1. The middle Eocene climatic optimum

A peak in warm/oligotrophic-water taxa is identified at

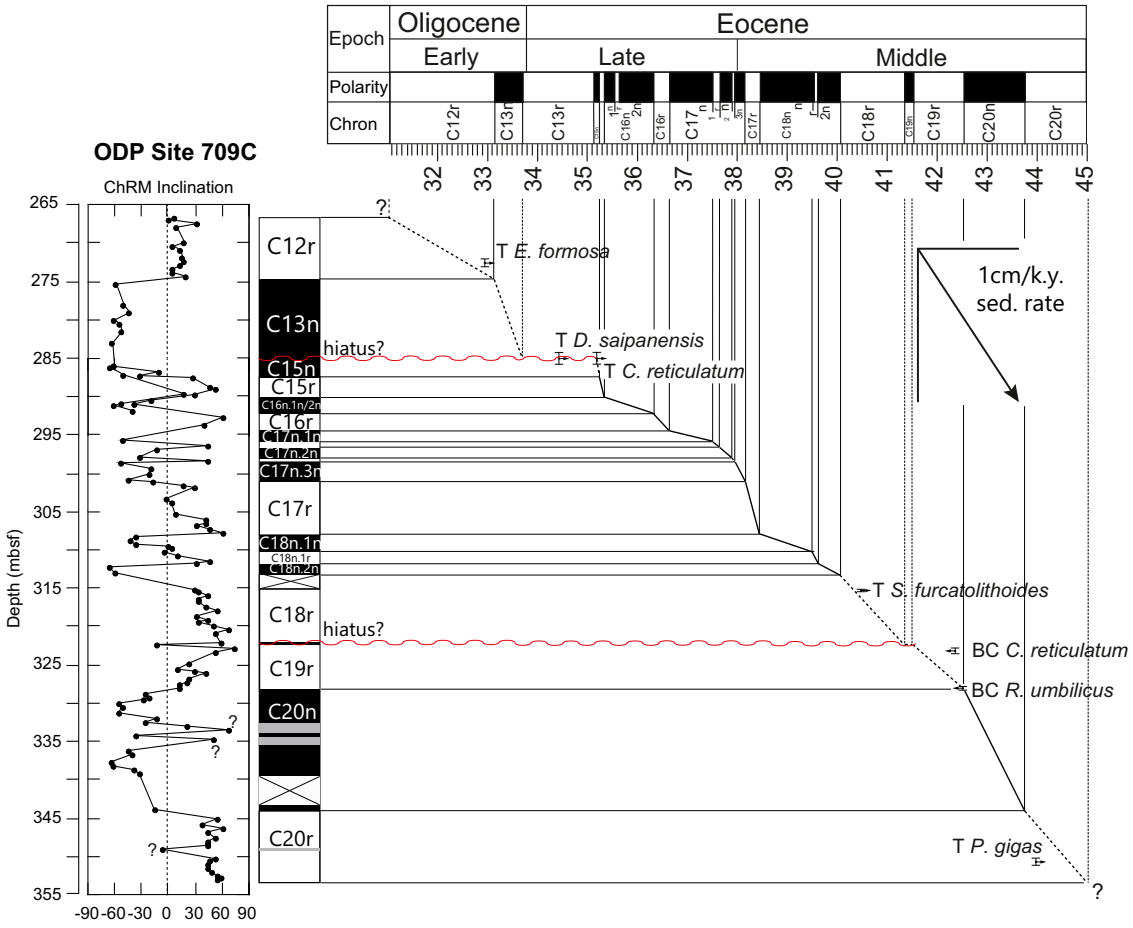

Fig. 6. Age vs. depth plot. Correlation between the polarity recognized at Hole 709C and the GPTS of Pälike et al., 2006 (Chron C12r to Chron C19n) and the geomagnetic polarity time scale of Cande and Kent, 1995 (Chron C20n and Chron C20r). Calcareous nannofossil datums are used to constrain the interpretation.

approximately 315 mbsf, corresponding to an age of about 40 Ma (Fig. 9). This timing is consistent with the MECO event (Jovane et al., 2007; Villa et al., 2008; Bohaty et al., 2009; Boscolo Galazzo et al., 2014) and represents the highest value in warm/oligotrophic taxa, before the beginning of the late Eocene cooling trend in which these taxa decrease prior to the EOT. The warm-water taxa peaks below this depth are consistent with the Eocene warm conditions and in particular at equatorial latitudes.

A core gap right above this depth prevents us from establishing if the MECO is extended upward. Furthermore, the extremely low resolution of the available $\delta^{18}O$ stable isotope data (Baker et al., 1990) precludes identification of this transient warming event, and future work should focus on obtaining a higher resolution of stable isotope chemostratigraphy. PCA factor 1 (variance 61%) fits well with the warm taxa curve, and we interpret that it records SST variation (Fig. 9).

3.5.2. *The Late Eocene climatic instability*

In the SO, at about 37 Ma a decrease of warm-water taxa has been evidenced and referred to as "Cooling C" (Villa et al., 2008) and later recognized as the Priabonian oxygen isotope maximum (PrOM, Scher et al., 2014, Pascher et al., 2015) which has been interpreted as a cooling event and which might be associated with a possible onset of widespread glaciation of Antarctica (Carter et al., 2017).

At equatorial latitude at Site 709 a weak response of this climatic event could be recognized as a decrease in warm-water taxa within Subchron C17n.1n.

3.5.3. *The Eocene - Oligocene transition*

Although the very low sedimentation rate makes data difficult to interpret, the decrease in warm/oligotrophic taxa from ~287 mbsf (about 35.2 Ma), is noteworthy. The change in the PCA Factor 2 toward negative values, at the base of Chron C15n is also noteworthy. As discussed in § 3.4, these modifications indicate a change in the surface nutrient regime, from oligotrophic to more eutrophic surface waters (Fig. 9). This result is related to the initiation of a proto-Antarctic Circumpolar Current (ACC) at ~35.5 Ma (Sarkar et al., 2019), as well as invigorated surface and bottom paleocurrents around Antarctica starting from about 35.7 Ma (Houben et al., 2019; Barker et al., 2007).

At 285 mbsf a relevant change in the nannofossil assemblage is identified and corresponds with a hiatus that juxtaposes upper Eocene taxa with common lower Oligocene eutrophic-taxa and indicating a reorganization of the sea surface nutrient regime. The hiatus includes at least the entire Chron C13r, and prevents the identification of the exact extent and position of the assemblage change. The hiatus has completely erased the reorganization of the nannofossil assemblage positioned at nearby Site 711 (Fioroni et al., 2015) in the late Eocene within Chron C13r between 34.5 and 34.1 Ma. This reorganization is also documented in Tanzania (Dunkley Jones et al., 2008), Java (Jones et al., 2019), and in the tropical Atlantic (Ravizza and Paquay, 2008). This assemblage variation indicates a measurable response of nannofossils to increased sea surface nutrient availability in the equatorial Indian Ocean and is possibly linked to the formation at high latitudes of nutrient-rich waters. In particular, the Subantarctic Mode Water (SAMW) is a water mass formed in the Southern Ocean by deep mixing, which sinks below the ocean surface and moves northward, carrying a large amount of regenerated nutrients to lower latitudes (Sarmiento et al., 2004). Changes in ocean paleocirculation, precursors of major glaciation at Oi-1, triggered enhanced mixing also at low latitudes, and consequently produced

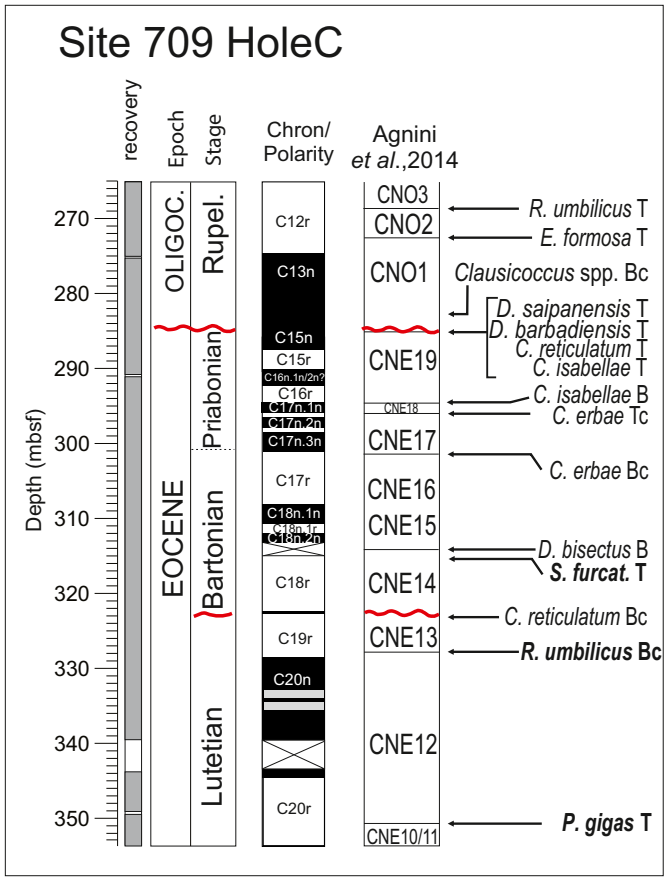

Fig. 7. Adopted biozonation and the position of the main biohorizons are plotted against magnetostratigraphy. Bioevents used as tie points are indicated in bold. T, B, Tc, Bc as explained in the text.

enhanced eutrophication of sea surface waters evidenced by nannofossil turnover, well before the EOT.

3.5.4. *The late Oligocene warming*

The lower resolution data set collected from ~270 to ~200 mbsf was analyzed to detect assemblage variations during the Oligocene. Warm and oligotrophic taxa, after the decrease at the EOT, show a gradual increase from about 240 mbsf (CNO4 Zone) (Fig. 10). We infer that this increase may reflect the globally recognized Late Oligocene Warming Event, previously detected in the Southern Ocean using nannofossil assemblage variation (Villa and Persico, 2006) and by oxygen isotopes (Pekar et al., 2006), and also recognized in other areas (e.g., Alegret et al., 2008; Wu et al., 2018).

4. Conclusions

The integrated calcareous nannofossil and magnetostratigraphic records from ODP Site 709C allow for the construction of a robust middle Eocene to late Oligocene chronostratigraphic framework. Despite the presence of two hiatuses in the middle Eocene and across the EOT, respectively, the ODP Site 709 record provides evidence of important changes in climate and paleoceanography at low latitudes during this critical time interval. Nannofossil assemblages record the MECO event (sensu Bohaty et al., 2009) including both the pre-MECO cooling and the warm peak at about 40 Ma.

A decline in warm water taxa following the MECO and up to about 37 Ma is reminiscent of the climatic instability recorded in this interval in the SO that includes the climatic deterioration of the "cooling B and C" events (~39 and ~37 Ma). This instability paved the way for the

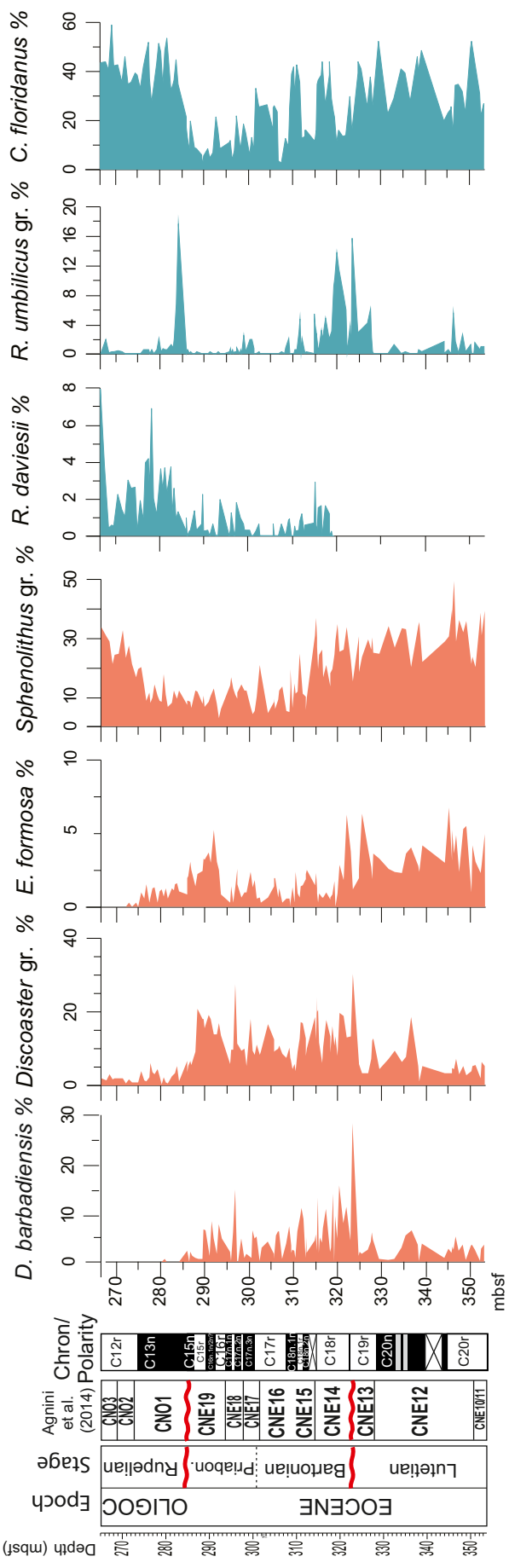

Fig. 8. Abundance pattern of selected taxa expressed as %, plotted against depth (mbsf) and magnetostratigraphy. The *Discoaster* group includes all the recognized species (*D. adamanteus, D. barbadiensis, D. bifax. D. saipanensis, D. tanii, Discoaster* sp.); the *Sphenolithus* group includes *S. akropodus, S. intercalaris, S. kempii, S. moriformis, S. obtusus, S. orphanknollensis, S. perpendicularis, S. predistentus, S. pseudoradians, S. quadrispinatus, S. radians, S. runus, S. spiniger, S. strigosus, S. tribulosus*, the *Reticulofenestra* group includes *R. umbilicus, R. samodurovi* and *R. dictyoda*.

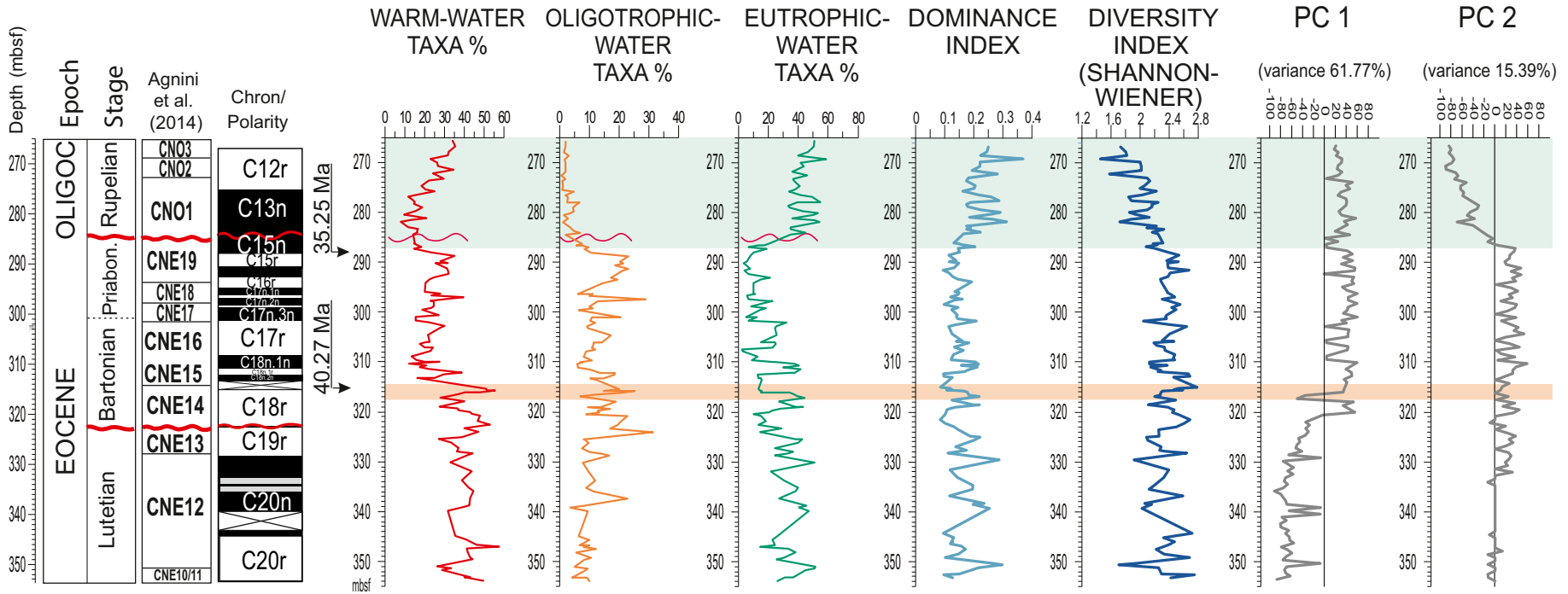

Fig. 9. Abundance pattern of middle Eocene to early Oligocene warm-water, oligotrophic, and eutrophic taxa plotted against depth (mbsf), magnetostratigraphy and biozones. Dominance and Shannon-Wiener indices, PC scores with respect to their corresponding nannofossil groups are shown. The pink line indicates the MECO event and the light green area indicates the late Eocene to early Oligocene eutrophic conditions. (For interpretation of the references to colour in this figure legend, the reader is referred to the web version of this article.)

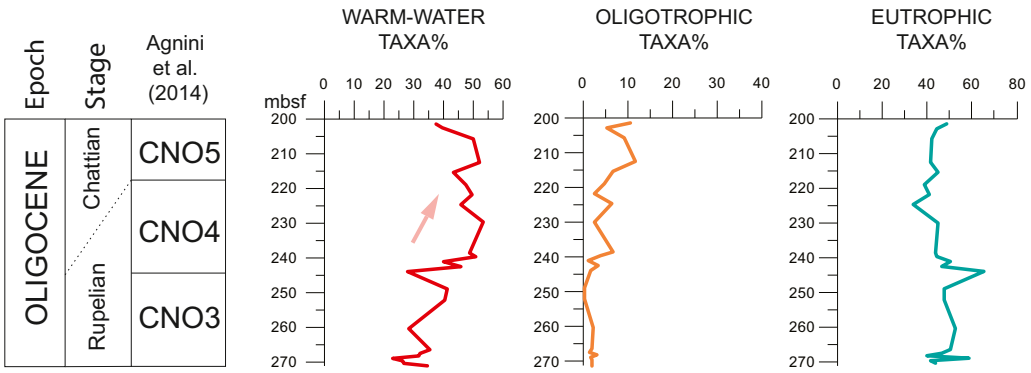

Fig. 10. Abundance pattern of early to late Oligocene warm, oligotrophic, and eutrophic taxa plotted against depth and biozones (Agnini et al., 2014). The arrow indicates the warming phase of the late Oligocene.

major climatic deterioration that occurred during the EOT. Prominent changes in Southern Ocean circulation related to the geographic isolation of Antarctica and invigorated bottom water currents in the late Eocene led to increased upwelling and enhanced nutrient supply at low latitudes. This change in nutrient supply is recorded in the shift from prevailing late Eocene oligotrophic to early Oligocene eutrophic assemblages.

An increase in warm water nannofossil taxa in the late Oligocene suggests a warming event at equatorial latitudes prior to the cooling at the Oligocene/Miocene boundary.

Declaration of Competing Interest

The authors declare that they have no known competing financial interests or personal relationships that could have appeared to influence the work reported in this paper.

Acknowledgements

We thank the Integrated Ocean Drilling Program (IODP) for providing access to the studied cores. The IODP is sponsored by the U.S. National Science Foundation (NSF) and participating countries under the management of Joint Oceanographic Institutions, Inc.

This work has benefited from the equipment and framework of the COMP-HUB Initiative, funded by the 'Departments of Excellence' programme of the Italian Ministry for Education, University and Research (MIUR, 2018–2022).

L.J. has been supported by Fundação de Amparo a Pesquisa do Estado de São Paulo (FAPESP) grant 2016/24946-9 and by the Coordenação de Aperfeiçoamento de Pessoal de Nível Superior - Brasil (CAPES) - Finance Code 001. We are grateful to Jean Self Trail for the careful revision and constructive suggestions. The authors strongly thank the editor Ric Jordan for thorough editing to the mnuscript.

Appendix A. Supplementary data

Supplementary data to this article can be found online at https://doi.org/10.1016/j.marmicro.2021.102051.

References

Agnini, C., Fornaciari, E., Raffi, I., Catanzariti, R., Pälike, H., Backman, J., Rio, D., 2014. Biozonation and biochronology of Paleogene calcareous nannofossils from low and middle latitudes. Newsl. Stratigr. 47, 131–181. https://doi.org/10.1127/0078-0421/2014/0042.

Alegret, L., Cruz, L.E., Fenero, R., Molina, E., Ortiz, S., Thomas, E., 2008. Effects of the Oligocene climatic events on the foraminiferal record from Fuente Caldera section (Spain, western Tethys). Palaeogeogr. Palaeoclimatol. Palaeoecol. 269, 94–102.

Arason, Þ., Levi, S., 2010. Maximum likelihood solution for inclination-only data in paleomagnetism. Geophys. J. Int. 182 (2), 753–771. https://doi.org/10.1111/j.1365-246X.2010.04671.x.

Aubry, M.P., 1992. Late Paleogene nannoplankton evolution: a tale of climatic deterioration. In: Prothero, D.R., Berggren, W.A. (Eds.), Eocene-Oligocene Climatic and Biotic Evolution. Princeton Univ. Press, Princeton, pp. 272–309.

Aubry, M.P., 1998. Early Paleogene calcareous nannoplankton evolution: a tale of climatic amelioration. In: Aubry, M.-P., Lucas, S.G., Berggren, W.A. (Eds.), Late Paleocene–Early Eocene Biotic and Climatic Events in the Marine and Terrestrial Records. Columbia University Press, New York, pp. 158–201.

Backman, J., Duncan, R.A., et al., 1988. Proc. ODP, Init. Repts, 115. Ocean Drilling Program, College Station, TX, pp. 459–588. https://doi.org/10.2973/odp.proc.ir.115.108.1988.

Backman, J., Raffi, I., Rio, D., Fornaciari, E., Palike, H., 2012. Biozonation and biochronology of Miocene through Pleistocene calcareous nannofossils from low and middle latitudes. Newsl. Stratigr. 45, 221–244. https://doi.org/10.1127/0078-0421/2012/0022.

Baker, P.A., Malone, M.J., Burns, S.J., Swart, P.K., 1990. Minor element and stable isotopic composition of the carbonate fine fraction: site 709, Indian Ocean. In: Duncan, R.A., Backman, J., Peterson, L.C., et al. (Eds.), Proc. ODP, Sci. Results, 1990. Ocean Drilling Program, 115: College Station, TX, pp. 661–675.

Barker, P.F., Filippelli, G.M., Florindo, F., Martin, E., Scher, H.D., 2007. Onset and role of the Antarctic circumpolar current. Deep-Sea Res. II Top. Stud. Oceanogr. 54, 2388–2398.

Bijl, P.K., Bendle, J.A., Bohaty, S.M., Pross, J., Schouten, S., Tauxe, L., Stickley, C.E., McKay, R.M., Röhl, U., Olney, M., 2013. Eocene cooling linked to early flow across the Tasmanian Gateway. P. Natl. Acad. Sci. USA 110, 9645–9650.

Bohaty, S.M., Zachos, J.C., 2003. Significant Southern Ocean warming event in the late middle Eocene. Geology 31, 1017–1020. https://doi.org/10.1130/G19800.1.

Bohaty, S.M., Zachos, J.C., Florindo, F., Delaney, M.L., 2009. Coupled greenhouse warming and deep-sea acidification in the middle Eocene. Paleoceanography 24, PA2207. https://doi.org/10.1029/2008PA001676.

Boscolo Galazzo, F., Thomas, E., Pagani, M., Warren, C., Luciani, V., Giusberti, L., 2014. The middle Eocene climatic optimum (MECO): a multiproxy record of paleoceanographic changes in the southeast Atlantic (ODP Site 1263, Walvis Ridge). Paleoceanography 29, 1143–1161. https://doi.org/10.1002/2014PA002670.

Bowles, J., 2007. Coring-related deformation of Leg 208 sediments from Walvis Ridge: implications for paleomagnetic data. Phys. Earth Planet. Inter. 161, 161–169.

Bown, P.R., Young, J.R., 1998. Techniques. In: Bown, P.R. (Ed.), Calcareous Nannofossil Biostratigraphy (British Micropalaeontological Society Publications Series). Chapman and Kluwer Academic, London, pp. 16–28.

Bown, P.R., Dunkley Jones, T., Lees, J.A., Pearson, P.N., Randell, R., Coxall, H.K., Mizzi, J., Nicholas, C., Karega, A., Singano, J., Wade, B.S., 2008. A calcareous microfossil Konservat Lagerstatte from the Paleogene Kilwa Group of coastal Tanzania. GSA Bull. 120, 3–12. https://doi.org/10.1130/B26261.1.

Bralower, T.J., 2002. Evidence of surface water oligotrophy during the Paleocene–Eocene thermal maximum: Nannofossil assemblage data from Ocean Drilling Program Site 690, Maud Rise, Weddell Sea. Paleoceanography 17 (2), 1023. https://doi.org/10.1029/2001PA000662.

Cande, S.C., Kent, D.V., 1995. Revised calibration of the geomagnetic polarity timescale for the Late Cretaceous and Cenozoic. J. Geophys. Res. 100, 6093–6095.

Cappelli, C., Bown, P.R., Westerhold, T., Bohaty, S.M., De Riu, M., Lobba, V., Yamamoto, Y., Agnini, C., 2020. The early to middle Eocene transition: an integrated calcareous nannofossil and stable isotope record from the Northwest Atlantic Ocean (IODP Site U1410). Paleoceanogr. Paleoclimatol. 34 (12), 1913–1930. https://doi.org/10.1029/2019PA003686.

Carter, A., Riley, T.R., Hillenbrand, C.-D., Rittner, M., 2017. Widespread Antarctic glaciation during the Late Eocene. Earth Planet. Sci. Lett. 458, 49–57. https://doi.org/10.1016/j.epsl.2016.10.045.

Cotton, L.J., Pearson, P., 2011. Extinction of larger foraminifera at the Eocene/Oligocene boundary. Palaeogeogr. Palaeoclimatol. Palaeoecol. 311 (3–4), 281–296. https://doi.org/10.1016/j.palaeo.2011.09.008.

Coxall, H.K., Pearson, P.N., 2007. The Eocene-Oligocene transition. In: Williams, M., et al. (Eds.), Deep-Time Perspectives on Climate Change: Marrying the Signal From Computer Models and Biological Proxies. Micropaleontology Society Special Publication London: Geological Society, pp. 351–387.

Coxall, H.K., Wilson, P.A., 2011. Early Oligocene glaciation and productivity in the eastern equatorial Pacific: insights into global carbon cycling. Paleoceanography 26, PA2221.
Coxall, H.K., Wilson, P.A., Pälike, H., Lear, C.H., Backman, J., 2005. Rapid stepwise onset of Antarctic glaciation and deeper calcite compensation in the Pacific Ocean. Nature 433 (7021), 53–57. https://doi.org/10.1038/nature03135.
Cronin, T.M., Cronin, M.A., 2015. Biological response to climate change in the Arctic Ocean: the view from the past. Arktos 1, 4. https://doi.org/10.1007/s41063-015-0019-3.
DeConto, R.M., Pollard, D., 2003. Rapid Cenozoic glaciation of Antarctica induced by declining atmospheric CO2. Nature 421, 245–249.
Dunkley Jones, T., Bown, P.R., Pearson, P.N., Wade, B.S., Coxall, H.K., Lear, C.H., 2008. Major shifts in calcareous phytoplankton assemblages through the Eocene-Oligocene transition of Tanzania and their implications for low-latitude primary production. Paleoceanography 23, 14. https://doi.org/10.1029/2008PA001640. PA4204.
Fioroni, C., Villa, G., Persico, D., Jovane, L., 2015. Middle Eocene-Lower Oligocene calcareous nannofossil biostratigraphy and paleoceanographic implications from Site 711 (equatorial Indian Ocean). Mar. Micropaleontol. 118, 50–62. https://doi.org/10.1016/j. marmicro.2015.06.001.
Fornaciari, E., Raffi, I., Rio, D., Villa, G., Backman, J., Olafsson, G., 1990. Quantitative distribution patterns of Oligocene and Miocene calcareous nannofossils from the western equatorial Indian Ocean. In: Duncan, R.A., Backman, J., Peterson, L.C., et al. (Eds.), Proceedings ODP, Scientific Results, 115. Ocean Drilling Program, College Station, TX, pp. 237–254. https://doi.org/10.2973/odp.proc.sr.115.153.
Fornaciari, E., Agnini, C., Catanzariti, R., Rio, D., Bolla, E.M., Valvasoni, E., 2010. Mid-latitude calcareous nannofossil biostratigraphy and biochronology across the middle to late Eocene transition. Stratigraphy 7 (4), 229–264. https://doi.org/10.1128/AAC.8.6.617.
Francis, J.E., Marenssi, S., Levy, R., Hambrey, M., Thorn, V.C., Mohr, B., Brinkhuis, H., Warnaar, J., Zachos, J., Bohaty, S., DeConto, R., 2009. From greenhouse to icehouse – the Eocene/Oligocene in Antarctica. In: Fabio Florindo and Martin Siegert, editors: Developments in Earth and Environmental Sciences, Vol 8, Antarctic Climate Evolution, Fabio Florindo and Martin Siegert, 2009. Elsevier, The Netherlands, pp. 309–368. https://doi.org/10.1016/S1571-9197(08)00008-6.
Fuller, M., Hastedt, M., Herr, B., 1998. Coring-induced magnetization of recovered sediment. In: Weaver, P.P.E., Schmincke, H.-U., Firth, J.V., Duffield, W. (Eds.), Proc. ODP, Sci. Res, 157. Ocean Drilling Program, College Station, TX, pp. 47–56.
Gibbs, S.J., Bralower, T.J., Bown, P.R., Zachos, J.C., Bybell, L.M., 2006. Shelf and open ocean calcareous phytoplankton assemblages across the Paleocene-Eocene thermal maximum: implications for global productivity gradients. Geology 34, 233–236. https://doi.org/10.1130/G22381.1.
Goldner, A., Herold, N., Huber, M., 2014. Antarctic glaciation caused ocean circulation changes at the Eocene-Oligocene transition. Nature 511 (7511), 574–577. https://doi.org/10.1038/nature13597.
Hammer, Ø., Harper, D.A.T., Ryan, P.D., 2001. PAST: Paleontological statistics software package for education and data analysis. Palaeontol. Electron. 4 (9), 1–9.
Hirt, A.M., Banin, A., Gehring, A.U., 1993. Thermal generation of ferromagnetic minerals from iron-enriched smectites. Geophys. J. Int. 115, 1161–1168.
Hooker, J.J., Collinson, M.E., Sille, N.P., 2004. Eocene-Oligocene mammalian faunal turnover in the Hampshire Basin, UK: calibration to the global time scale and the major cooling event. J. Geol. Soc. 161 (2), 161–172. https://doi.org/10.1144/0016-764903-091.
Houben, A.J.P., Bijl, P.K., Sluijs, A., Schouten, S., Brinkhuis, H., 2019. Late Eocene Southern Ocean cooling and invigoration of circulation preconditioned Antarctica for full-scale glaciation. Geochem. Geophys. Geosyst. 20, 2214–2234. https://doi.org/10.1029/2019GC008182.
Hrouda, F., 1994. A technique for the measurement of thermal changes of magnetic susceptibility of weakly magnetic rocks by the CS-2 apparatus and KLY-2 Kappabridge. Geophys. J. Int. 118, 604–612.
Hutchinson, D.K., Coxall, H.K., Lunt, D.J., Steinthorsdottir, M., de Boer, A.M., Baatsen, M., von der Heydt, A., Huber, M., Kennedy-Asser, A.T., Kunzmann, L., Ladant, J.-B., Lear, C.H., Moraweck, K., Pearson, P.N., Piga, E., Pound, M.J., Salzmann, U., Scher, H.D., Sijp, W.P., Śliwińska, K.K., Wilson, P.A., Zhang, Z., 2021. The Eocene-Oligocene transition: a review of marine and terrestrial proxy data, models and model-data comparisons. Clim. Past 17, 269–315. https://doi.org/10.5194/cp-17-269-2021.
Jones, A.P., Dunkley Jones, T., Coxall, H., Pearson, P.N., Nala, D., Hoggett, M., 2019. Low-latitude calcareous nannofossil response in the Indo-Pacific Warm Pool across the Eocene-Oligocene Transition of Java, Indonesia. Paleoceanogr. Paleoclimatol. 34, 1833–1847. https://doi.org/10.1029/2019PA003597.
Jovane, L., Florindo, F., Coccioni, R., Dinares-Turell, J., Marsili, A., Monechi, S., Roberts, A.P., Sprovieri, M., 2007. The middle Eocene climatic optimum event in the Contessa Highway section, Umbrian Apennines, Italy. Geol. Soc. Am. Bull. 119 (3), 413–427. https://doi.org/10.1130/B25917.1.
Kalb, A.L., Bralower, T.J., 2012. Nannoplankton origination events and environmental changes in the late Paleocene and early Eocene. Mar. Micropaleontol. 92, 1–15. https://doi.org/10.1016/j.marmicro.2012.03.003.
Kennedy-Asser, A.T., Lunt, D.J., Farnsworth, A., Valdes, P.J., 2019. Assessing mechanisms and uncertainty in modelled climatic change at the Eocene-Oligocene transition. Paleoceanogr. Paleoclimatol. 34, 16–34. https://doi.org/10.1029/2018PA003380.
Kennett, J.P., 1977. Cenozoic evolution of Antarctic glaciation, circum-Antarctic ocean, and their impact on global paleoceanography. J. Geophys. Res. 82, 3843–3860.
Lagabrielle, Y., Goddéris, Y., Donnadieu, Y., Malavieille, J., Suarez, M., 2009. The tectonic history of Drake Passage and its possible impacts on global climate. Earth Planet. Sci. Lett. 279, 197–211. https://doi.org/10.1016/j.epsl.2008.12.037.
Liu, Z., Pagani, M., Zinniker, D., Deconto, R.M., Huber, M., Brinkhuis, H., et al., 2009. Eocene-Oligocene climate transition. Science (New York, N.Y.) 323 (February), 1187–1190. https://doi.org/10.1126/science.1166368.
Lurcock, P.C., Florindo, F., 2019. New developments in the Puffin Plot paleomagnetic data analysis program. Geochem. Geophys. Geosyst. 20, 5578–5587. https://doi.org/10.1029/2019GC008537.
Miller, K.G., Fairbanks, R.G., Mountain, G.S., 1987. Tertiary oxygen isotope synthesis, sea-level history and continental margin erosion. Paleoceanography 2, 1–19.
Miller, K.G., Browning, J.V., Aubry, M.P., Wade, B.S., Katz, M.E., Kulpecz, A.A., Wright, J.D., 2008. Eocene-Oligocene global climate and sea-level change: St. Stephens Quarry, Alabama. GSA Bull. 120, 34–53. https://doi.org/10.1130/B26105.1.
Okada, H., 1990. Quaternary and Paleogene calcareous nannofossils, Leg 115. In: Duncan, R.A., Backman, J., Peterson, L.C., et al. (Eds.), Proceedings ODP Scientific Results, 115. Ocean Drilling Program, College Station, TX, pp. 129–174.
Pagani, M., Zachos, J.C., Freeman, K.H., Tipple, B., Bohaty, S.M., 2005. Marked decline in atmospheric carbon dioxide concentrations during the Paleogene. Science 309, 600–603. https://doi.org/10.1126/science.1110063.
Pagani, M., Huber, M., Liu, Z., Bohaty, S.M., Henderiks, J., Sijp, W., et al., 2011. The role of carbon dioxide during the onset of antarctic glaciation. Science 334 (6060), 1261–1264. https://doi.org/10.1126/science.1203909.
Pälike, H., Norris, R.D., Herrle, J.O., Wilson, P.A., Coxall, H.K., Lear, C.H., Shackleton, N. J., Tripati, A.K., Wade, B.S., 2006. The heartbeat of the Oligocene climate system. Science 314, 1894–1898. https://doi.org/10.1126/science.1133822.
Pälike, H., Lyle, M., Nishi, H., Raffi, I., Gamage, K., Klaus, A., the Expedition 320/321 Scientists, 2010. Proc. IODP, 320/321. Integrated Ocean Drilling Program Management International, Inc., Tokyo https://doi.org/10.2204/iodp.proc.320321.2010.
Pälike, H., Lyle, M.W., Nishi, H., Raffi, I., Ridgwell, A., Gamage, K., Baldauf, J., et al., 2012. A Cenozoic record of the equatorial Pacific carbonate compensation depth. Nature 488, 609–614. https://doi.org/10.1038/nature11360.
Pascher, K.M., Hollis, C.J., Bohaty, S.M., Cortese, G., McKay, R.M., Seebeck, H., Suzuki, N., Chiba, K., 2015. Expansion and diversification of high-latitude radiolarian assemblages in the late Eocene linked to a cooling event in the southwest Pacific. Clim. Past 11, 1599–1620. www.climpast.net/11/1599/2015/. https://doi.org/10.5194/cp-11-1599-2015.
Pekar, S.F., DeConto, R., Harwood, D.M., 2006. Resolving a late Oligocene conundrum: deep-sea warming versus Antarctic glaciation. Palaeogeogr. Palaeoclimatol. Palaeoecol. 231, 29–40. https://doi.org/10.1016/j.palaeo.2005.07.024.
Persico, D., Villa, G., 2004. Eocene–Oligocene calcareous nannofossils from Maud Rise and Kerguelen Plateau/Antarctica: Paleoecological and paleoceanographic implications. Mar. Micropaleontol. 52, 153–179. https://doi.org/10.1016/j.marmicro.2004.05.002.
Ravizza, G., Paquay, F., 2008. Os isotope chemostratigraphy applied to organic rich marine sediments from the Eocene-Oligocene transition on the West African margin (ODP Site 959). Paleoceanography 23, PA2204. https://doi.org/10.1029/2007PA001460.
Rio, D., Raffi, I., Villa, G., 1990. Pliocene-Pleistocene calcareous nannofossil distribution patterns in the western Mediterranean. In: Kastens, K., Mascle, J., et al. (Eds.), Proc. ODP, Sci. Results, 107. Ocean Drilling Program, College Station, TX, pp. 513–533.
Sarkar, S., Basak, C., Frank, M., Berndt, C., Huuse, M., Badhani, S., Bialas, J., 2019. Late Eocene onset of the Proto-Antarctic circumpolar current. Nat. Sci. Rep. 9, 10125. https://doi.org/10.1038/s41598-019-46253-1.
Sarmiento, J.L., Gruber, N., Brzezinski, M.A., Dunne, J.P., 2004. High-latitude controls of thermocline nutrients and low latitude biological productivity. Nature 427, 56–60.
Savian, J.F., Jovane, L., Bohaty, S.M., Wilson, P.A., 2013. Middle Eocene to early Oligocene magnetostratigraphy of ODP Hole 711A (Leg 115), western equatorial Indian Ocean. Geol. Soc. Lond. Spec. Publ. 373, 97–110. https://doi.org/10.1144/SP373.16.
Savian, J.F., Jovane, L., Giorgioni, M., Iacoviello, F., Rodelli, D., Roberts, A.P., Chang, L., Florindo, F., Sprovieri, M., 2016. Environmental magnetic implications of magnetofossil occurrence during the Middle Eocene Climatic Optimum (MECO) in pelagic sediments from the equatorial Indian Ocean. Palaeogeogr. Palaeoclimatol. Palaeoecol. 441, 212–222. https://doi.org/10.1016/j.palaeo.2015.06.029.
Scher, H.D., Bohaty, S.M., Smith, B.W., Munn, G.H., 2014. Isotopic interrogation of a suspected late Eocene glaciation. Paleoceanography 29, 628–644. https://doi.org/10.1002/2014PA002648.
Schneider, D.A., Kent, D.V., 1990. Paleomagnetism of Leg 115 sediments: implications for Neogene magnetostratigraphy and paleolatitude of the Réunion Hotspot. In: Duncan, R.A., Backmann, J., Peterson, L.C., et al. (Eds.), Proceedings of the Ocean Drilling Program, Scientific Results, 115. Ocean Drilling Program, College Station, TX, pp. 717–736. https://doi.org/10.2973/odp.proc.sr.115.197.1990.
Shipboard Scientific Party, 1988. Site 709. In: Backman, J., Duncan, R.A., et al. (Eds.), Proc. ODP, Init. Repts, 115. Ocean Drilling Program, College Station, TX, pp. 459–588. https://doi.org/10.2973/odp.proc.ir.115.108.1988.
Torsvik, T.H., Van der Voo, R., Preeden, U., MacNiocaill, C., Steinberger, B., Doubrovine, P., et al., 2012. Phanerozoic polar wander, palaeogeography and dynamics. Earth Sci. Rev. 114, 325–368.
Touchard, Y., Rochette, P., Aubry, M.P., Michard, A., 2003. High-resolution magnetostratigraphic and biostratigraphic study of Ethiopian traps-related products in Oligocene sediments from the Indian Ocean. Earth Planet. Sci. Lett. 206, 493–508.
Van Andel, T.H., 1975. Mesozoic/Cenozoic calcite compensation depth and the global distribution of calcareous sediments. Earth Planet. Sci. Lett. 26, 187–194.
van Hinsbergen, D.J., de Groot, L.V., van Schaik, S.J., Spakman, W., Bijl, P.K., Sluijs, A., Langereis, C.G., Brinkhuis, H., 2015. A Paleolatitude calculator for paleoclimate studies (model version 2.1). PLoS One 10, 1–21.

Villa, G., Persico, D., 2006. Late Oligocene climatic changes: evidence from calcareous nannofossils at Kerguelen Plateau Site 748 (Southern Ocean). Palaeogeogr. Palaeoclimatol. Palaeoecol. 231, 110–119. https://doi.org/10.1016/j.palaeo.2005.07.028.

Villa, G., Fioroni, C., Pea, L., Bohaty, S.M., Persico, D., 2008. Middle Eocene–late Oligocene climate variability: Calcareous nannofossil response at Kerguelen Plateau, Site 748. Mar. Micropaleontol. 69, 173–192. https://doi.org/10.1016/j.marmicro.2008.07.006.

Villa, G., Fioroni, C., Persico, D., Roberts, A.R., Florindo, F., 2014. Middle Eocene to Late Oligocene Antarctic glaciation/deglaciation and Southern Ocean productivity. Paleoceanography 29, 223–237. https://doi.org/10.1002/2013PA002518.

Wade, B., Pearson, P., 2008. Planktonic foraminiferal turnover, diversity fluctuations and geochemical signals across the Eocene/Oligocene boundary in Tanzania. Mar. Micropaleontol. 68, 244–255. https://doi.org/10.1016/j.marmicro.2008.04.002.

Wei, W., Villa, G., Wise Jr., S.W., 1992. Paleoceanographic implications of Eocene-Oligocene calcareous nannofossils from Sites 711 and 748 in the Indian Ocean. In: Wise Jr., S.W., Schlich, R., et al. (Eds.), Proc. ODP. Scientific Results, 120, pp. 979–999.

Westerhold, T., Marwan, N., Drury, A.J., Liebrand, D., Agnini, C., Anagnostou, E., Barnet, J.S.K., Bohaty, S.M., De Vleeschouwer, D., Florindo, F., Frederichs, T., Hodell, D.A., Holbourn, A.E., Kroon, D., Lauretano, V., Littler, K., Lourens, L.J., Lyle, M., Pälike, H., Röhl, U., Tian, J., Wilkens, R.H., Wilson, P.A., Zachos, J.C., 2020. An astronomically dated record of Earth's climate and its predictability over the last 66 million years. Science 369, 6509,1383–1387. https://doi.org/10.1126/science.aba6853.

Winter, A., Siesser, W.G., 1994. Coccolithophores. Cambridge Univ. Press, Cambridge, p. 242.

Wu, F., Miao, Y., Meng, Q., Fang, X., Sun, J., 2018. Late Oligocene Tibetan Plateau warming and humidity: evidence from a sporopollen record. Geochem. Geophys. Geosyst. 20, 434–441. https://doi.org/10.1029/2018GC007775.

Zanazzi, A., Kohn, M.J., MacFadden, B.J., Terry, D.O., 2007. Large temperature drop across the Eocene-Oligocene transition in central North America. Nature 445, 639–642.

Zijderveld, J.D.A., 1967. A. C. demagnetization of rocks: analysis of results. In: Collinson, D.W., Creer, K.M., Runcorn, S.K. (Eds.), Methods in Palaeomagnetism, Dev. in Solid Earth Geophys. Elsevier, Amsterdam, pp. 254–286.